Energy 66 (2014) 860–867

Contents lists available at ScienceDirect

Energy

journal homepage: www.elsevier.com/locate/energy

Reducing energy consumption of a steam ejector through experimental optimization of the nozzle geometry

Navid Sharifi [a,*], Majid Sharifi [b]

[a] Department of Aerospace Engineering, Amirkabir University of Technology, Hafez Ave., No. 424, P.O. Box: 15875-4413, Tehran, Iran
[b] Department of Chemical and Biological Engineering, Drexel University, Philadelphia, USA

ARTICLE INFO

Article history:
Received 17 July 2013
Received in revised form
10 January 2014
Accepted 16 January 2014
Available online 11 February 2014

Keywords:
Energy consumption
Steam ejector
Experimental optimization
CFD simulation
Supersonic nozzle

ABSTRACT

Steam ejectors use pressurized vapor as the motive flow for running in steam cycles. The major parameter that affects the thermal energy consumption is the pressure of motive flow used in this device. In the current study, a malfunctioning experimental ejector is studied numerically to reveal the source of low evacuation rate from a suction chamber. This ejector was designed to operate under a motive pressure of 6 bar. However, the required vacuum in the suction vessel was not attained unless the pressure of motive steam was increased to 8 bar. The fastest and the most inexpensive way of improving the device performance was considered as replacing just the primary nozzle, with no further changes in ejector's body because, the ejector was connected to other unit facilities and hence the ejector replacement was very costly. The optimization procedure was performed through using numerical CFD (Computational Fluid Dynamics) simulations. The shape of internal supersonic nozzle was changed in many CFD analyses and the most optimized nozzle was selected for manufacturing. After installing the designed nozzle, an improved entrainment capability under the nominal pressure of 6 bar was observed and the desired vacuum level was attained.

1. Introduction

MED (multi-effect distillation) is one of desalination methods in which a series of condensation–evaporation processes is taking place in a nearly vacuum condition. The objective of this process is to provide a low-pressure condition inside evaporators to be able to evaporate water at considerably low temperatures [1]. It not only promotes the efficiency of the desalination process, but also prevents the formation of salinity on tube bundles leading to unchanging values for heat transfer coefficients. At such conditions, the total energy required to evaporate seawater will be substantially decreased [2].

Apart from using the mechanical driven pumps, there is an alternate way to evacuate the air from the system interior. The alternative that is frequently used in desalination systems is to use ejectors. The principle of this method is to entrain the internal air via a supersonic jet flow. Ejectors that are used in desalination facilities are particularly designed to produce higher vacuum levels. These types of ejectors might be driven by air or steam. Recently, some process enhancement by integrating optimal steam ejectors were developed which allows a 10–25% reduction in the amount of valuable steam [3].

Fig. 1 shows a schematic diagram of the steam cycle in a conventional desalination unit. A package of serial evaporators, a condenser, an ejector, and a thermo-compressor are used to recycle the steam to the system. As seawater vaporizes in the system, dissolved air and non-condensable gases are evolved. These gases should be vented to prevent over-pressurizing of the system. The ejector draws the mixture of non-condensable gases from the condenser as the secondary flow. This process causes the seawater to evaporate at lower pressure conditions in the system and thus, less thermal energy is required. The discharge flow of the ejector (i.e. the mixture of primary and secondary flows) is exhausted into the atmosphere.

The remainder non-condensable vapors in the condenser are recycled to the first stage evaporator via a thermal vapor compressor. Although large-scale ejectors i.e. thermo-compressors play a significant role in such systems, they are not investigated herein.

Since the performance of ejectors is controlled by the thermodynamic states of entrained and motive flows, the pressure of motive steam affects the ejector performance significantly.

* Corresponding author. Tel.: +98 912 4980125; fax: +98 216 6959020.
E-mail addresses: sharifinavid@aut.ac.ir, sharifinavid@yahoo.com (N. Sharifi).

0360-5442/$ – see front matter © 2014 Elsevier Ltd. All rights reserved.
http://dx.doi.org/10.1016/j.energy.2014.01.055

Nomenclature

English letters

A	section area (m^2)
D	diameter (m)
E	total energy (J)
g	gravitational acceleration (m^2/s)
k	thermal conductivity (W/m K)
L	length (m)
$\dot{m}$	mass flow rate (kg/s)
M	Mach number (Dimensionless)
P	static pressure (Pa)
r	radial coordinate (m)
T	static temperature (K)
u	velocity components (m/s)
x	independent variable (−)
y	dependent variable (−)
z	axial coordinate (m)
CR	compression ratio (Dimensionless)
ER	entrainment ratio (Dimensionless)

Greek letters

α	converging angle (deg)
κ	turbulence kinetic energy (m^2/s^2)
ε	turbulence dissipation rate (m^2/s^3)
ρ	density (kg/m^3)
θ	tangential coordinate (deg)
τ	stress tensor (Pa)
μ	dynamic viscosity (Pa s)

Subscripts

d	diffuser flow (−)
p	primary flow (−)
s	secondary flow (−)

Therefore, steam consumption and interior vacuum level are strongly related to a proper ejector design. This paper will primarily focus on the effect of nozzle geometry on ejector's performance.

The productive studies based on classical one-dimensional theory for ejectors have been continuously carried out since 1950 [4]. Nowadays, flow visualization methods are frequently used for determining the complicated flow pattern inside ejectors. Though the well-known internal phenomena have been revealed by CFD (Computational Fluid Dynamics) methods to estimate the real flow properties in steam ejectors, the deep-concealed mixing mechanisms within these devices are still ambiguous and need more efforts to investigate. The works done by Riffat et al. [5,6] could be mentioned as the first CFD studies performed on ejectors. Some numerical studies in supersonic ejectors were supported with appropriate experimental data [7,8]. The results of such numerical methods were used to optimize the mechanical design of ejectors [9–11]. CFD studies concerned about turbulence modeling revealed that the two-equation turbulence theories (such as k–ε and k–ω models) may be best suited to represent the mixing and compressing phenomena in ejectors [12].

Rusly et al. [13] performed several simulations on ejectors using finite volume techniques to resolve the flow dynamics in the ejectors. During their validation steps, it was found that predicted entrainment ratios from CFD data had a greater accuracy on definite area ratios of the device. Although, they were recorded no shock wave in their ejector.

Kouhikamali et al. [14] presented a numerical method for large size ejectors used in desalination systems called thermo-compressor. They could experimentally modify the entrainment ratio of a malfunctioning thermo-compressor through using some CFD simulations which were performed to visualize the flow streamlines and vortices in the mixing zone.

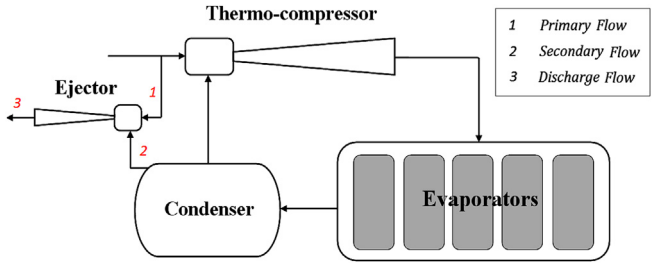

Fig. 1. Schematic of flow diagram in a thermal distillation system equipped with a steam ejector.

Some valuable numerical attempts made to produce applicable design curves for estimating the converging angle of mixing zone of ejectors [15]. These graphs were used to optimize the casing geometry of conventional ejectors.

Some parametric studies were conducted by Yari et al. [16] to optimize the performance of novel ejector-expansion cascade refrigeration cycles under various operating conditions. The proposed cycles exhibited a reasonable value of coefficient of performance with a much less value of discharge temperature, compared to the conventional cycles.

A recent study [17,18] on comparing different CFD approaches (i.e. 2D and 3D numerical modeling) was performed on the actual shape of ejectors, in order to consider non-symmetrical effects of flow bending inside the suction pathway. The results showed a considerable difference and were outlined in applicable design methodologies for optimizing the geometry of vapor compressors which could deliver a high amount of suction steam at the discharge boundary.

Ji et al. [19] focused on the effects of operating pressure and ejector geometry on the flow structure and the performance of a steam ejector. The converging angle of the duct considered the geometrical parameter in their study and was varied from 0.5 to 4.5 deg. After validating their numerical simulations with available experimental test case, they found that the ejector with a converging duct angle of 1 deg. had the best performance.

The reasons of obtaining the numerical results outside the experimental data in some ranges of operating conditions of ejectors were discussed thoroughly in Ref. [20]. Since the behavior of steam flow in the supersonic nozzle used in the main body of ejectors is doubtful to be a single-phase phenomenon, a novel two-phase simulation was performed according to recent development in wet-steam theory [21]. It was found that the entrainment ratio of a vapor compressor is significantly increased according to occurrence of condensation shock in the motive steam. This resultant could be used for further energy analysis in order to reduce the required motive energy for running a high-performance ejector.

In the current study, an existing in-site ejector is adjusted through modifying its nozzle geometry such that an elevated rate of suction flow is attained under ejector's nominal operating condition.

2. Background and ejector theory

A schematic view of a steam ejector is shown in Fig. 2. As the high pressure steam (i.e. primary flow) accelerates through the primary nozzle, it expands with supersonic speed and generates a very low pressure region at the nozzle exit plane (i.e. in the mixing chamber). The pressure difference between the two fluids causes the surrounding fluid (i.e. secondary flow), to be entrained into the mixing chamber and mixed with the motive flow. The mixed supersonic flow will be further decelerated in the converging zone and its speed reduces to nearly sonic values where a strong shock wave is taking place. This shock wave causes a sudden drop in the flow speed (i.e. from supersonic to subsonic), and a major compression process is taken place. A further compression of the flow mixture will be achieved as it passes through the subsonic diffuser.

Several parameters could be used to describe the performance of an ejector. For evacuation applications, the most important ones are “compression ratio” and “entrainment ratio”.

$$\mathrm{ER} = \frac{\dot{m}_s}{\dot{m}_p} \tag{1}$$

$$\mathrm{CR} = \frac{P_d}{P_s} \tag{2}$$

The entrainment ratio is related to the energy efficiency of ejectors and the compression ratio limits the pressure at which the secondary flow can be ejected. The variations of these parameters in a typical ejector are plotted in Fig. 3. It shows the performance curve of a typical ejector at a constant value of motive pressure. This graph is obtained by calculating the values of entrainment ratio at different values of compression ratio.

Referring to eq. (2), an increase in the value of compression ratio could be obtained either by lowering the secondary pressure or raising the discharge pressure. The key to obtain a performance curve in a steam ejector is that the discharge pressure is determined by boundary conditions and thus is a constant value (i.e. the ambient pressure). Therefore, the only way to obtain an increased compression ratio level is to reduce the secondary flow pressure.

As observed, there are two different zones on this simple graph. These regions refer to distinct operational conditions of ejectors which will be thoroughly explained in Section 5.

3. Problem specifications

A schematic of experimental ejector used in the system and its nozzle are shown in Fig. 4 to demonstrate the position of internal supersonic nozzle in the ejector body. This ejector was designed to operate under nominal pressure of 6 bar. However, this level of motive pressure was not able to produce the required vacuum level

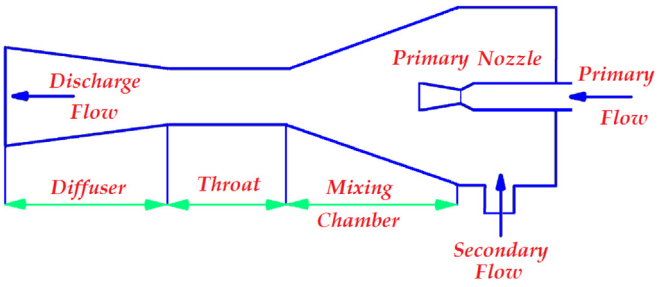

Fig. 2. Schematic of different zones and flows in a conventional ejector.

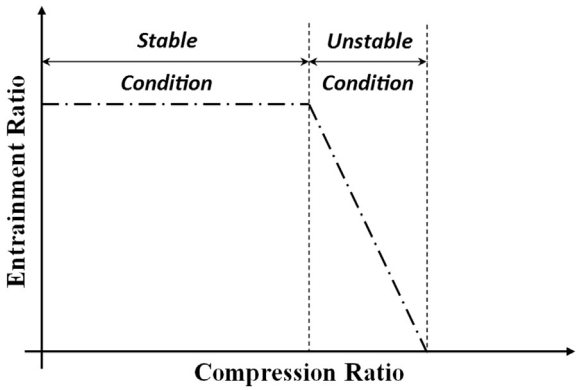

Fig. 3. Performance curve of a conventional ejector.

in the desalination system until the motive flow pressure raised to 8 bar.

Since the motive flow accelerates to sonic speed inside the throat of the nozzle, the steam flow rate can be calculated assuming the choked condition in the throat. The mass flow of a compressible flow through the choked throat can be expressed as a function of upstream flow properties.

$$\dot{m} = \left(\frac{P_0 A}{\sqrt{RT_0}}\right)\left[M\sqrt{\gamma}\left(1+\frac{\gamma-1}{2}M^2\right)^{\frac{\gamma+1}{2-2\gamma}}\right] \tag{3}$$

Considering the sonic velocity condition (i.e. $M = 1$) at the throat, constant specific heat capacity ($\gamma = 1.3$) for water vapor, measured values of P_0, T_0 and known throat cross-section area (A), this relation can be used to estimate the maximum mass flow rate ($\dot{m}$) which can be passed through a given area section.

According to eq. (3), the mass flow rate of the motive steam directly depends on the upstream pressure (i.e. P_0) and thus, increasing the flow pressure leads to over-consumption of the motive flow in the nozzle of the ejector. Therefore, the undesired surpassing mass flow rate of the primary steam from the nominal consumption rate provoked us to design a new ejector layout in order to produce the required vacuum level in the suction chamber under the corresponding consumption rate considered for this device (i.e. 6 bar).

4. Numerical procedure

The compressible flow within the ejector is modeled using the Navier–Stokes equations, based on the conservation of mass, momentum and energy. This set of equations is solved by a control volume approach in the CFD commercial package FLUENT 6.3.

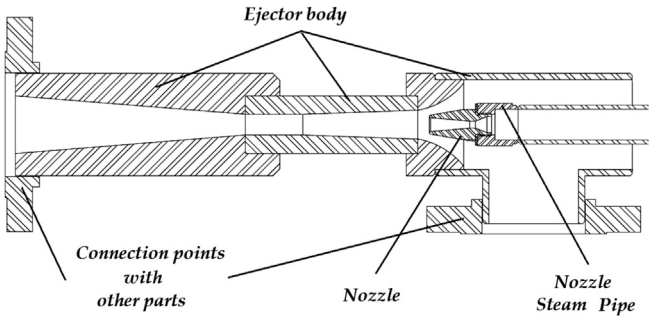

Fig. 4. Experimental ejector with connections to other parts of the desalination system.

4.1. Governing equations

Although the mixing of the two streams is a three-dimensional phenomenon, the flow behavior along major parts of the ejector could be approximately predicted through using axisymmetric models. Therefore, the cylindrical forms of flow equations of motion are used to model the axisymmetric flow within the ejector. In this respect, the governing equations can be rewritten in the subsequent forms.

$$\frac{\partial \rho}{\partial t}+\frac{1}{r}\frac{\partial}{\partial r}(\rho r u_r)+\frac{\partial}{\partial z}(\rho u_z)=0 \tag{4}$$

$$\rho\left(\frac{\partial u_r}{\partial t}+u_r\frac{\partial u_r}{\partial r}-\frac{u_\theta^2}{r}+u_z\frac{\partial u_r}{\partial z}\right)= -\frac{\partial p}{\partial r}+\rho g_r+\mu\left[\frac{\partial}{\partial r}\left(\frac{1}{r}\frac{\partial (r u_r)}{\partial r}\right)+\left(\frac{\partial^2 u_r}{\partial z^2}\right)\right] \tag{5}$$

$$\rho\left(\frac{\partial u_\theta}{\partial t}+u_r\frac{\partial u_\theta}{\partial r}-\frac{u_r u_\theta}{r}+u_z\frac{\partial u_\theta}{\partial z}\right)= \rho g_\theta+\mu\left[\frac{\partial}{\partial r}\left(\frac{1}{r}\frac{\partial}{\partial r}(r u_\theta)\right)+\left(\frac{\partial^2 u_\theta}{\partial z^2}\right)\right] \tag{6}$$

$$\rho\left(\frac{\partial u_z}{\partial t}+u_r\frac{\partial u_z}{\partial r}+u_z\frac{\partial u_z}{\partial z}\right)= -\frac{\partial p}{\partial z}+\rho g_z+\mu\left[\frac{1}{r}\frac{\partial u}{\partial r}\left(r\frac{\partial u_z}{\partial r}\right)+\left(\frac{\partial^2 u_r}{\partial z^2}\right)\right] \tag{7}$$

$$\frac{\partial}{\partial t}(\rho E)+\nabla\cdot[\vec{u}(\rho E+p)]=\nabla\cdot[(k\nabla T)+(\tau\nabla T)] \tag{8}$$

where the divergence terms in the axisymmetric form is:

$$\nabla\cdot\vec{u}=\frac{1}{r}\frac{\partial}{\partial r}(r u_r)+\frac{\partial}{\partial z}(u_z) \tag{9}$$

The equations were discretized using the second order upwind scheme, and solved using FLUENT's implicit coupled density-based scheme. The accuracy of the numerical solution was examined by comparing results obtained with different spatial discretization schemes, different grid resolutions. Negligible difference was observed between the various discretization schemes and meshes.

It is necessary to consider an appropriate turbulence model since the mixing phenomenon of two streams takes place in a viscous flow region and cannot be treated by simplified inviscid or viscous-inviscid interaction schemes. The k–ε turbulence model is selected herein while the standard near wall function is used for the near wall treatment. The *realizable* k–ε model which is an improved version of the conventional *standard* k–ε theory is employed in this study. This is due to its capability in predicting more accurate spreading rate of a round jet [22].

$$\frac{\partial}{\partial t}(\rho\kappa)+\frac{\partial}{\partial x_i}(\rho\kappa u_i)=\frac{\partial}{\partial x_j}\left[\left(\mu+\frac{\mu_t}{\sigma_\kappa}\right)\frac{\partial \kappa}{\partial x_j}\right]+\mathrm{Src}_\kappa \tag{10}$$

$$\frac{\partial}{\partial t}(\rho\varepsilon)+\frac{\partial}{\partial x_i}(\rho\varepsilon u_i)=\frac{\partial}{\partial x_j}\left[\left(\mu+\frac{\mu_t}{\sigma_\varepsilon}\right)\frac{\partial \varepsilon}{\partial x_j}\right]+\mathrm{Src}_\varepsilon \tag{11}$$

where, the mentioned source terms (Src_κ, Src_ε) can be found in Ref. [22].

4.2. Boundary conditions

There are two distinct flows entering the ejector beside a single outgoing stream. The inlet type boundary condition with known total pressure and temperature was applied to both entering boundaries, while the outlet type boundary condition with known static pressure was applied to the boundary of discharge flow. These values are depicted in Table 1 and assumed fixed during all CFD calculations.

It should be noted that, the outgoing flow is subsonic and the exit pressure for subsonic outflow would be sufficient to perform numerical calculations, while the rest of the flow parameters (i.e. temperature and mass flow rate) are extrapolated from the interior of the computational domain.

4.3. Grid generation and geometry

The computational grid approximately consists of uniformly sized quadrilateral elements, with 35 grid cells in the radial direction and about 1050 grid cells in the axial direction in the ejector domain, and 1200 (i.e. 15 × 80) additional grid cells in the primary nozzle region. Moreover, dense meshes are present in the mixing chamber around the exit plane of the primary nozzle due to occurrence of complex mixing phenomena which have a great influence on the whole flow pattern in the ejector. The geometry consists of a primary nozzle mounted on the centerline of the ejector body as shown in Fig. 4.

The main dimensions of the ejector body and the primary nozzle are listed in Table 2. The distance between the primary nozzle and the inlet of the mixing chamber is kept constant during all following alterations.

5. Results and discussion

5.1. Verification of computational procedure

In order to verify the numerical procedure, it is necessary to provide the results and compare with other computational studies performed on ejectors. Since the presence of shock wave plays a major role in the compression phenomenon in such devices, it is a good criterion to be represented and discussed about.

Fig. 5 shows the contours of Mach number within the ejector which is considered in this study. The flow pattern shows a supersonic jet exited from the nozzle outlet with a mach number

Table 1
Temperature and pressure values of ejector boundaries.

	Temperature	Pressure
Primary flow	175 °C	6 bar
Secondary flow	55 °C	20 kPa
Discharge flow	–	100 kPa

Table 2
Dimensions of the ejector body.

	Item	Size (mm)
Primary nozzle	Nozzle inlet diameter	30
	Nozzle throat diameter	15
	Nozzle outlet diameter	35
	Nozzle length	148
Body	Converging length	212
	Constant length	93
	Diffuser length	415
	Pipe distance from the mixing chamber	17
	Body throat diameter	83

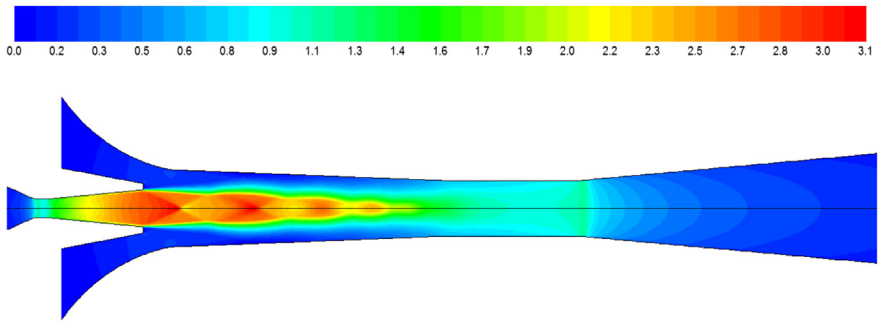

Fig. 5. Contours of Mach number within the example ejector at nominal motive pressure.

around 3 and extended into the throat of the ejector. Fig. 6(a) and (b) represents the results of two other numerical studies performed on supersonic jet ejectors used by Pianthong et al. [9] and Rusly et al. [13].

These figures show a similar layout inside ejectors which demonstrate a shock wave close to the diverging zone at the end zone of the ejector throat. The flow downstream of the shock wave is all subsonic with a considerably higher pressure value than suction pressure.

It should be noted that, the difference in the range of Mach number in these models is due to different motive flow pressures used for running ejectors.

5.2. Analyzing the malfunctioning ejector

Firstly, it is necessary to numerically investigate the sources of low compression ratio values in the ejector at nominal operating conditions. As mentioned earlier, in order to obtain the performance curve in a wide range of compression ratios, the suction pressure was gradually increased, whilst the discharge pressure was kept constant. The resultant of this procedure is shown in Fig. 7. This graph enables us to clearly explain the transient behavior of the ejector in evacuation process.

At the beginning, both suction and discharge sides are at atmospheric pressure level (i.e. 1 bar) and therefore, compression is not happening at this stage. But, large momentum of the motive flow exited from the nozzle causes the secondary flow to be continuously entrained by the ejector. This phenomenon makes the pressure of the secondary flow to drop down the ambient pressure level and thus, the compression ratio of the ejector starts to go up gradually. In this operational mode, the ejector is operating at a stable condition and the entrainment ratio is staying unchanged during the evacuation process. The “stable” zone on the performance graph (zone A) represents this operating state.

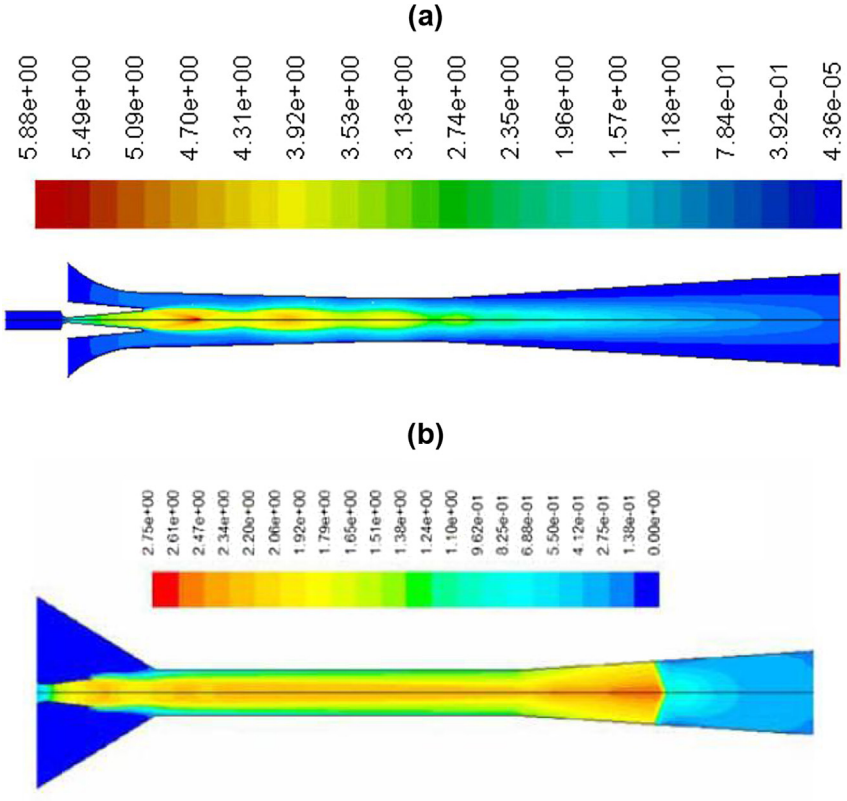

Fig. 6. Contours of Mach number inside other studied ejectors from literature, (a) ejector used by Pianthong et al. [9], (b) ejector used by Rusly et al. [13].

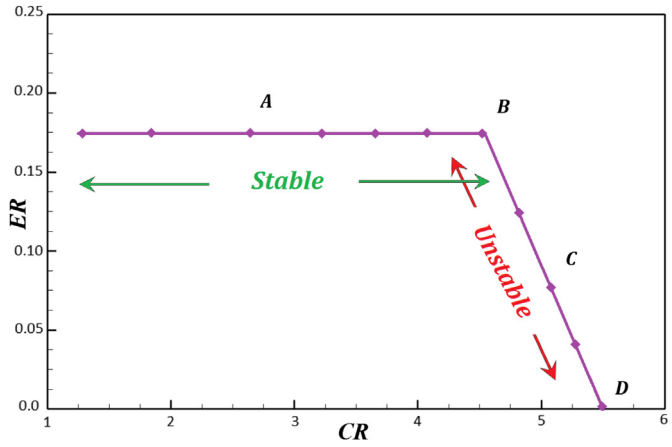

Fig. 7. Numerical performance curve of the ejector at nominal motive pressure.

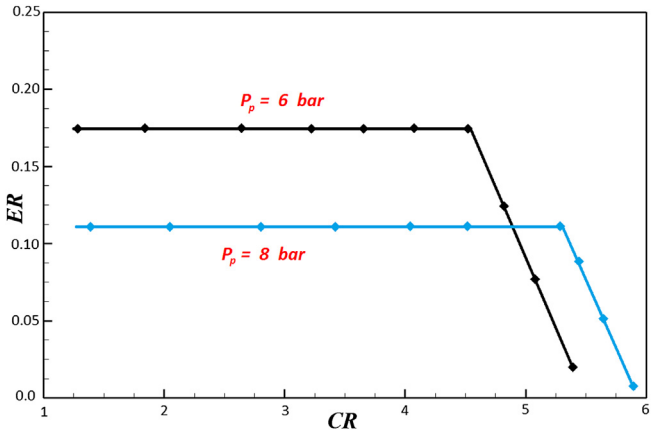

Fig. 8. Numerical performance curves of the ejector at different motive pressures.

This phenomenon continues to the point where a critical compression ratio (point B) on performance curve is attained. This point shows the highest capability of the ejector to suck the secondary flow from the chamber (i.e. interior space of the desalination unit).

After this critical point which is known as MDP (maximum discharge point), the entrainment ratio is dropped quickly. The inclined section on the performance graph (zone C) represents this unstable condition. This point (MDP) simply means that higher compression ratio is just attainable through delivering lower mass flow rates. Besides, this region is not a stable operational mode and the entrainment ratio is experimentally fluctuates between 0.2 and 0.5 (i.e. the delivered mass flow rate is reduced significantly). Therefore, zone C is considered as the unstable operational mode for the ejector.

Point D shows the minimum entrainment ratio above which the motive flow reverse back to the suction chamber and the ejector is known to be operating at reverse-flow condition. This undesired condition could pressurize the interior parts of the system which should be rigorously avoided.

As a result, the horizontal zone on the performance graph is considered as the desirable operating condition of ejectors, where the highest value of the compression ratio (i.e. point B) is considered as the reliable compression ratio.

5.3. The effect of motive pressure on the performance

Referring to boundary conditions mentioned in Section 4, the required values of compression ratio should at least 5 to produce the desired vacuum level in suction chamber (i.e. the condenser and other interior parts of the system). As illustrated in Fig. 7, the attainable value of compression ratio under the nominal value of motive pressure (i.e. 6 bar) is lower than 5. Therefore, current motive flow is not able to produce the sufficient vacuum level in the unit.

Since the critical compression ratio is lower than the desired value, the pressure of motive steam is temporarily increased to 8 bar to provide an elevated critical compression ratio and to obtain the required vacuum level in the suction chamber. Now, it is necessary to compare the numerically obtained performance curves and explore the detailed phenomena in these situations. Then, propose a modification method based on the results of these two graphs.

Fig. 8 displays the performance curves under two motive pressure values (i.e. 6 and 8 bar). As seen, the compression ratio of the ejector (i.e. MDP) is substantially increased at $P = 8$ bar, because motive steams with higher energy level are injected to the ejector at higher pressure conditions and hence, the compression capability of the device is strengthened.

In contrast, the corresponding entrainment ratio at $P = 8$ bar is significantly decreased. The reason is related to the lower rate of motive flow passed through the choked nozzle based on eq. (3). Hence, the ratio of the suction to the motive flow rate is decreased according to eq. (2).

This means that the total steam consumption for producing the desired vacuum level is substantially increased (in the choked nozzle), which further lead a significant amount of energy to be wasted. Therefore, it is necessary to optimize the ejector to operate exactly at the nominal motive pressure.

5.4. Study of the nozzle profile

There are many possible ways to attain an appropriate design for modifying a malfunctioning ejector. Since the geometry of the ejector has the most influence on the performance of the device, the possible solution for improving the compression ratio is to construct new ejectors with different geometries.

For the currently installed ejector, replacement of the ejector body is very costly due to renewing all junctions, pipes and facilities coupled with it. Therefore, it was decided to modify and design a more efficient nozzle for the ejector instead. This procedure is feasibly simpler and more inexpensive as the ejector repairing cost is not included. The goal is to attain the desired vacuum level at suction chamber via the nominal values of motive pressure of 6 bar.

The nozzle geometry has a significant influence on the flow field within the ejector since the supersonic jet core exiting the nozzle outlet plane strongly depends on the flow pattern throughout the nozzle. Therefore, it could be possible to obtain a specific nozzle geometry that produces a modified flow field in the ejector and optimizes the ejector's performance.

Referring to Fig. 4, the sketch of the nozzle is illustrated with detailed dimensions in Fig. 9. As seen, major dimensions in the profile of the nozzle are:

- The converging length (L_1)
- The diverging length (L_2)
- The inlet diameter (D_1)
- The inlet diameter (D_2)
- The throat diameter (D_{th})

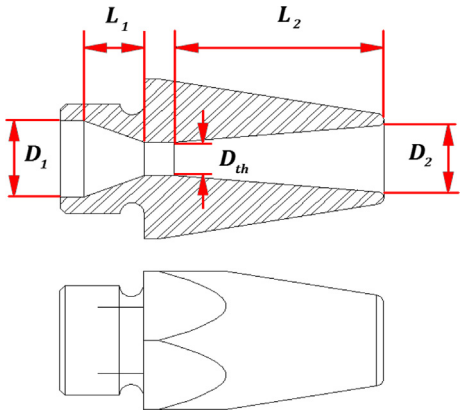

Fig. 9. Sketch of the primary nozzle with dominant dimensions on the cross-section.

These dimensions for different nozzle geometries are listed in Table 3. The obtained profiles were used to produce the whole geometry for the ejector and generate appropriate grid elements inside the domain. Afterwards, the numerical simulation was performed and the results were compared. The objective of this numerical study is to obtain a nozzle profile which produces the required compression ratio (i.e. at least 5 for this application) with the largest entrainment ratio.

All the numerical simulations were constrained to a constant inlet diameter (D_1) and throat diameter (D_{th}). The inlet diameter should be designed such that it fits the steam pipe (in Fig. 4). Throat diameter has also kept constant as it has a direct influence on the steam consumption rate. The performance parameters have been further computed at the nominal pressure of 6 bar. Values of compression ratio and entrainment ratio for these ten profiles are given in Table 4.

It should be noted that, the larger ER (entrainment ratio) values denote the higher suction flow rate in the ejector. Moreover, the desirable compression ratio for evacuating the system is around 5. Therefore, the CR (compression ratio) value should be the first parameter to meet the requirements (must be equal or greater than 5).

Then, among profiles that are having acceptable values of compression ratio, the ones with larger ER values are preferred, as they provide higher suction flow rate and result in reduced evacuation time.

Fig. 10 shows the comparative performance curves of these profiles in the ejector under study. As observed more clearly, the performance curve of the 9th nozzle is the best one suited for this purpose because, it offers the CR value of 5.27 which is above the required compression ratio, while the corresponding ER value (i.e. 0.155) is higher than other estimated ER values.

Table 3
Dimensions of the nozzle profiles.

Profile	L_1 (mm)	L_2 (mm)	D_1 (mm)	D_2 (mm)	D_{th} (mm)
1	30	130	30	36	15
2	30	150	30	36	15
3	30	140	30	38	15
4	40	140	30	36	15
5	30	120	30	36	15
6	40	145	30	34	15
7	30	140	30	32	15
8	40	130	30	36	15
9	30	130	30	36	15
10	30	150	30	38	15

Table 4
Computational performance parameters of the ejector with different nozzle profiles.

Profile	CR	ER
1	4.82	0.118
2	5.23	0.151
3	4.95	0.137
4	5.05	0.144
5	4.68	0.105
6	5.09	0.147
7	5.14	0.151
8	5.00	0.143
9	5.27	0.155
10	5.18	0.145

The profile of this item was selected as the design basis for manufacturing the nozzle. Both nozzles (i.e. the first installed nozzle and the modified nozzle) are shown in Fig. 11(a) and (b).

A considerable improvement in the ejector performance was observed after installation of this nozzle. The experimental vacuum level after installation of modified nozzle was measured in-site and improved suction capability of the ejector was observed. The results showed a more acceptable vacuum level (i.e. around 10 kPa) after replacing the modified nozzle.

6. Conclusion

A malfunctioning ejector was studied numerically to find sources of low compression ratio values. The existing in-site motive flow could not afford the required vacuum level in suction chamber. In addition, any modification in ejector design was rejected due to the large capital cost attributed to unit shut down, ejector replacement, installation and further services. Therefore, investigations are dedicated toward design modifications of nozzle geometry instead. 10 different nozzle profiles were designed, where they are all constrained to both constant inlet and throat diameter. The characteristic curves for each of the ejectors obtained, and among all, the one surpasses the required CR value i.e. 5 while yields the highest entrainment ratio is chosen as the optimized nozzle geometry. The nozzle was manufactured and installed in-site. The observed experimental value for vacuum pressure was in good agreement with the values obtained from numerical models indicating the success of resolving the ejector malfunctioning issue with a simple nozzle replacement.

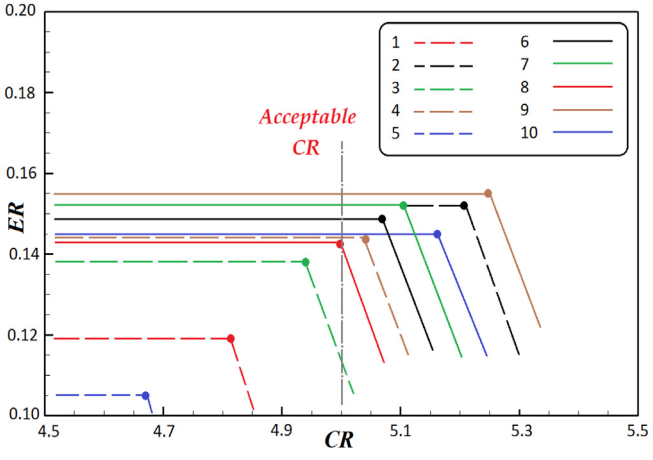

Fig. 10. Numerical performance curves of different nozzle profiles.

(a)

(b)

Fig. 11. Experimentally manufactured nozzles for the steam ejector, (a) first malfunctioning nozzle, (b) optimized nozzle based on CFD results.

Acknowledgment

The authors wish to thank Fan-Niroo Company for its help to construct the experimental ejector model and the permission to publish their records.

References

[1] Adel M, Dayem A. Experimental and numerical performance of a multi-effect condensation–evaporation solar water distillation system. Energy 2006;31:2710–27.
[2] Sharaf MA, Nafey AS, Rodriguez LG. Thermo-economic analysis of solar thermal power cycles assisted MED–VC (multi effect distillation–vapor compression) desalination processes. Energy 2011;36:2753–64.
[3] Reddick C, Sorin M, Rheault F. Energy savings in CO_2 (carbon dioxide) capture using ejectors for waste heat upgrading. Energy 2014;65:200–8.
[4] Sun DW. Variable geometry ejectors and their applications in ejector refrigeration systems. Energy 1996;21:919–29.
[5] Riffat SB, Gan G, Smith S. Computational fluid dynamics applied to ejector heat pumps. Appl Therm Eng 1996;16:291–7.
[6] Riffat SB, Omer SA. CFD modeling and experimental investigation of an ejector refrigeration system using methanol as the working fluid. Int J Energy Resour 2001;25:115–28.
[7] Desevaux P, Aeschbacher O. Numerical and experimental flow visualization of the mixing process inside an induced air ejector. Int J Turbo Jet Engine 2002;19:71–8.
[8] Sriveerakul T, Aphornratana S, Chunnanond K. Performance prediction of steam ejector using computational fluid dynamics: part 1. Validation of the CFD results. Int J Therm Sci 2007;46:812–22.
[9] Pianthong K, Seehanam W, Behnia M, Sriveerakul T, Aphornratana S. Investigation and improvement of ejector refrigeration system using computational fluid dynamics technique. Energy Convers Manag 2007;48:2556–64.
[10] Chaiwongsa P, Wongwises S. Experimental study on R-134a refrigeration system using a two-phase ejector as an expansion device. Appl Therm Eng 2008;28:467–77.
[11] Yapıcı R, Ersoy HK, Aktoprakoglu A, Halkacı HS, Yigit O. Experimental determination of the optimum performance of ejector refrigeration system depending on ejector area ratio. Int J Refrig 2008;31:1183–9.
[12] Bartosiewicz Y, Aidoun Z, Mercadier Y. Numerical assessment of ejector operation for refrigeration applications based on CFD. Appl Therm Eng 2006;26(5–6):604–12.
[13] Rusly E, Aye L, Charters WWS, Ooi A. CFD analysis of ejector in a combined ejector cooling system. Int J Refrig 2005;28:1092–101.
[14] Kouhikamali R, Sharifi N. Experience of modification of thermo-compressors in multiple effects desalination plants in Assaluyeh in IRAN. Appl Therm Eng 2012;40:174–80.
[15] Sharifi N, Boroomand M, Sharifi M. Numerical optimization of ejector geometry based on non-dimensional parameters, ASME 2012. In: International mechanical engineering congress & exposition, IMECE2012–86837.
[16] Yari M, Mahmoudi SMS. Thermodynamic analysis and optimization of novel ejector-expansion TRCC (transcritical CO_2) cascade refrigeration cycles (novel transcritical CO_2 cycle). Energy 2011;36:6839–50.
[17] Sharifi N, Boroomand M. An investigation of thermo-compressor design by analysis and experiment: part 1. Validation of the numerical method. Energy Convers Manag 2013;69:217–27.
[18] Sharifi N, Boroomand M. An investigation of thermo-compressor design by analysis and experiment: part 2. Development of design method by using comprehensive characteristic curves. Energy Convers Manag 2013;69:228–37.
[19] Ji MK, Utomob T, Woo JS, Lee YH, Jeong HM, Chung HS. CFD investigation on the flow structure inside thermo vapor compressor. Energy 2010;35:2694–702.
[20] Sharifi N, Boroomand M, Sharifi M. Numerical assessment of steam nucleation on thermodynamic performance of steam ejectors. Appl Therm Eng 2013;52:449–59.
[21] Sharifi N, Boroomand M, Kouhikamali R. Wet steam flow energy analysis within thermo-compressors. Energy 2012;47:609–19.
[22] FLUENT 6.3 User's guide. FLUENT INC.: Lebanon, NH, USA.